Mon. Not. R. Astron. Soc. **000**, 0–0 (0000) Printed 18 November 1997 (MN plain TEX macros v1.6)

Density cusps: restrictions on non-axisymmetric models

D. Syer
Max-Planck-Institut für Astrophysik, 85740 Garching-bei-München, Germany.

HongSheng Zhao
Sterrewacht Leiden, Niels Bohr Weg 2, Leiden, The Netherlands.

ABSTRACT
Galactic nuclei are now generally thought to have density cusps in their centres, and the evidence is mounting that as a consequence they are unlikely to be triaxial. Self-consistent stellar dynamical models of non-axisymmetric cusps would be an interesting counter-argument to this conclusion. We consider 2-d analogues of triaxial cusps: a sequence of non-axisymmetric, cuspy discs first described by Sridhar & Touma (1997). Scale-free models with potential $\Phi \propto r^{\alpha}$ are examined in detail. It is shown analytically for $0 < \alpha \lesssim 0.43$ that self-consistent models with positive phase-space density *do not* exist. Numerical solutions of the combined Vlasov and Poisson equations suggest that the *whole* sequence of models with $0 < \alpha < 1$ are also unphysical. Together with existing work on cusps, we conclude on purely theoretical grounds that galactic nuclei are not expected to be triaxial.

Key words: galaxies: kinematics and dynamics

1 INTRODUCTION

The intrinsic shape of elliptical galaxies is a long-standing problem, the solution to which may help us to understand the process of galaxy formation. Dissipationless collapse and merger models predict that ellipticals should generally be triaxial with slow figure rotation and anisotropic velocity ellipsoids (van Albada 1982, Dubinski & Carlberg 1991, Navarro, Frenk & White 1996). But there is no strong observational evidence for triaxiality (Merritt 1996). Results from deprojection of light—fitting stellar kinematics and statistical analysis of the flattening vs. misalignment—are inconclusive (Franx, Illingworth & de Zeeuw 1992, Statler 1994). In particular, one cannot yet rule out the possibility that all ellipticals are either prolate or oblate.

One purely theoretical approach to the problem is to examine whether equilibrium models with strong triaxiality exist. Recent observations of the central region of ellipticals have found that the luminosity density rises as a power-law at small radius (Crane *et al.* 1993, Gebhardt *et al.* 1996). Schwarzschild (1993) shows that models with strong cusp and strong triaxiality cannot be in equilibrium for much longer than the diffusion time of the chaotic orbits. This is because the regular box orbits are destroyed by the high density at the centre. The boxlets such as banana and fish orbits are not enough to make a self-consistent model without the chaotic orbits. Similar study of 2-d non-axisymmetric models by Kuijken (1993) reaches similar conclusions. Merritt & Fridman (1996) discuss 3-d cuspy models which are not scale free, and also reach similar conclusions.

In this paper we examine the existence of cuspy, non-axisymmetric models using a new sequence of Stäckel models by Sridhar & Touma (1997). These models in their simplest form are self-similar. They are also 2-dimensional, and as such would not make good models for 3-d galactic nuclei. Their interest lies in the fact that they are minimally symmetric, and hence represent the 2-d analogue of a triaxial system. Also very important is the fact that they admit only regular orbits, which makes their interpretation much simpler. Sridhar & Touma (1997) postulate that, since banana orbits are elongated in the direction supporting the flattened potential, self-consistent realizations of the models could exist. If true, this would be a counter example to the results of previous work on non-axisymmetric cusps, and one could argue that galactic nuclei may indeed be triaxial.

After a brief review of the known results of the models of Sridhar & Touma (1997) in Section 2, we formulate the problem of testing self-consistency in Section 3. Analytical results and numerical results are given in Sections 4 and 5, and Section 6 concludes.

2 THE STÄCKEL POTENTIAL

2.1 Co-ordinates

It is convenient to switch between two different coordinate systems. In the usual polar coordinates (r, θ), one can define a new parabolic co-ordinate system (ξ,η),

$$\xi = r(\cos\theta + 1),\quad \eta = r(\cos\theta - 1), \tag{1}$$

so that curves of constant ξ or constant η are orthogonal parabolas.

2.2 Potential

In the absence of a central black hole, the self-similar potential of Sridhar & Touma (1997) is

$$\Phi = \tfrac{1}{2} r^\alpha [(1+\cos\theta)^{1+\alpha} + (1-\cos\theta)^{1+\alpha}], \quad \alpha \in (0,1), \tag{2}$$

where in their notation we have set $2K = 1$ and $\gamma = 1-\alpha$.

This potential is in Stäckel form when written in terms of the parabolic co-ordinates:

$$\Phi = \frac{\xi^{1+\alpha} + \eta^{1+\alpha}}{\xi - \eta}, \tag{3}$$

or

$$\Phi = \frac{F_+(\xi) - F_-(\eta)}{\xi - \eta} \tag{4}$$

where

$$F_+(\xi) = \xi^{1+\alpha} \tag{5},$$

and

$$F_-(\eta) = -F_+(|\eta|). \tag{6}$$

The potential (2) and the corresponding surface density Σ we write as

$$\Phi(r,\theta) = r^\alpha P(\theta),\quad \Sigma(r,\theta) = r^{\alpha-1} S(\theta). \tag{7}$$

where

$$P(\theta) = \tfrac{1}{2}[(1+\cos\theta)^{1+\alpha} + (1-\cos\theta)^{1+\alpha}]. \tag{8}$$

The functions $S(\theta)$ and $P(\theta)$ are related by Poisson's equation, which can be written as

$$S(\theta) = \int_0^\infty \int_0^{2\pi} \mathrm{d}w \mathrm{d}\phi \; w^{\alpha-1} \frac{\alpha^2 P(\phi) + P''(\phi)}{[1 + w^2 - 2w\cos(\phi-\theta)]^{1/2}}. \tag{9}$$

where primes represent differentiation (see Sridhar & Touma 1997) and we set $4\pi^2 G = 1$.

As a consequence of (4), the dynamics in the (r,θ) plane is analytic. There are two conserved quantities: the energy E and a second classical integral I, given by

$$\begin{aligned} I &= 2\xi p_\xi^2 - \xi E + F_+(\xi) \\ &= 2\eta p_\eta^2 - \eta E + F_-(\eta), \end{aligned} \tag{10}$$

where (p_ξ, p_η) are the conjugate momenta to (ξ,η). The orbits of particles are bounded by the co-ordinate lines. The shapes of two orbits are shown for illustrative purposes in Figure 1.

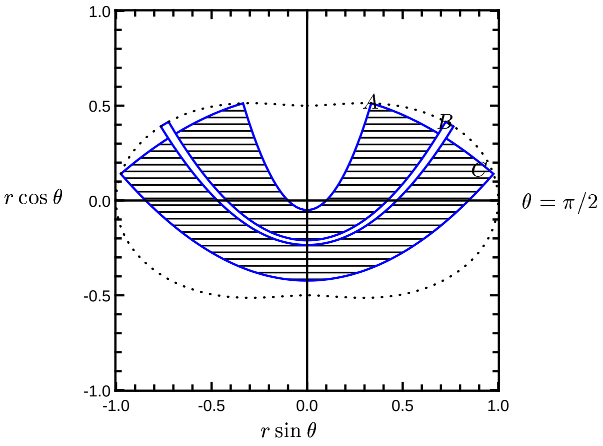

Figure 1. The region covered by two orbits in the model with $\alpha = 0.5$. Both orbits have $E = 1$; the fat one has $I = 0.0684$ ($y/y_{\max} = 0.462$), and the thin one has $I = 0.1478$ ($y/y_{\max} = 0.998$). Orbits with negative y are upside-down version of these ones: mirror images reflected in $\theta = \pi/2$. The zero velocity surface $E = \Phi$ is shown as a dotted line, on which the symbols A and C mark the turning points of the fat orbit; B marks the ends of the thin orbit.

3 TESTING SELF-CONSISTENCY

3.1 Dynamics

By Jeans' Theorem, the distribution function is $f(E,I)$, and the associated surface density can be written

$$\Sigma(r,\theta) = \int f(E,I)\mathrm{d}^2 v. \tag{11}$$

The element of phase space in terms of E and I can be derived by equating

$$\mathrm{d}p_\xi \mathrm{d}p_\eta \mathrm{d}\xi \mathrm{d}\eta = \mathrm{d}^2 v \mathrm{d}^2 r \tag{12}$$

which is true by virtue of the fact that (p_ξ, p_η) are conjugate momenta. Hence

$$\mathrm{d}^2 v = \frac{1}{r} \frac{\partial(\xi,\eta)}{\partial(r,\theta)} \frac{\partial(p_\xi,p_\eta)}{\partial(E,I)} \mathrm{d}E \mathrm{d}I. \tag{13}$$

Now from equation (1)

$$\frac{\partial(\xi,\eta)}{\partial(r,\theta)} = 2r\sin\theta \tag{14}$$

and from equation (10)

$$2\sin\theta \frac{\partial(p_\xi,p_\eta)}{\partial(E,I)} = \frac{1}{2\sqrt{(I-I_-)(I_+-I)}} \tag{15}$$

where

$$I_+ = -E\eta + F_-(\eta),\quad I_- = -E\xi + F_+(\xi). \tag{16}$$

Thus

$$2\Sigma(r,\theta) = \int f(E,I) \frac{\mathrm{d}E \mathrm{d}I}{\sqrt{(I-I_-)(I_+-I)}}, \tag{17}$$

where the integration is over the range of (E,I) for which the integrand in real: $I \in [I_-, I_+]$ ($I_+ > I_-$ is implied by $E \geq \Phi$).

3.2 Self-similarity

Self-similarity implies that the distribution function can be written in the form

$$f = E^{-\frac{1}{\alpha}} g(IE^{-1-1/\alpha}). \tag{18}$$

Thus, defining

$$Q \equiv \frac{2S}{P^{1-1/\alpha}}. \tag{19}$$

and setting $z = \Phi/E$ and $y = IE^{-1-1/\alpha}$, the integral relating Σ and f (equation 17) can be written

$$Q(\theta) = \int z^{1/\alpha-2} g(y) \frac{\mathrm{d}z\mathrm{d}y}{\sqrt{(y-y_-)(y_+-y)}} \tag{20}$$

where $y_\pm$ are defined in the Appendix. (The fact that Q comes out independent of r is *a posteriori* proof that equation (18) was the correct form for the distribution function.)

The region of integration in equation (20) is that bounded by the curves $y = y_\pm(z, \theta)$. It is illustrated in Figure 2.

The maximum value of $|y|$ is given by the turning point of y_+ with respect to variations in z and θ. It is easy to show by differentiation that the maximum is

$$y_{\max} = \frac{\alpha}{(1+\alpha)^{1+1/\alpha}}. \tag{21}$$

The orbits of particles with $y = \pm y_{\max}$ are along the co-ordinate lines, and hence are thin bananas (cf Bishop 1987)—parabolic thin shells with their tips lying on the surface $E = \Phi$. Note that the largest value of y in the shaded region in Figure 2 is less than $y_{\max}$, and hence there is no thin banana with $y > 0$ for $\alpha = 0.5$, $\theta = \pi/3$. The smallest value of y is however $-y_{\max}$, so there is a thin banana with $y < 0$.

3.3 Self-consistency

The problem we would like to solve is to find a distribution function which self-consistently generates the density and the potential in equation (7); i.e. we seek $g(y)$ such that $S(\theta)$ is given by equations (20) and (19), with Poisson's equation (9) simultaneously satisfied.

Since the model density is symmetric about $\theta = 0$ *and* $\pi/2$, we should always weight equally a banana orbit and its reflection in $\theta = \pi/2$; thus $g(y)$ is even, and we need only consider positive y. We define K_+ as the contribution to Q from a single positive value of y:

$$K_+(\theta, y) = \int z^{1/\alpha-2} \frac{\mathrm{d}z}{\sqrt{(y-y_-)(y_+-y)}}. \tag{22}$$

The corresponding quantity K_- for negative y is just the reflection of K_+ in the major axis, $\theta = \pi/2$:

$$K_-(\theta, y) = K_+(\pi - \theta, -y). \tag{23}$$

For each value of θ there is a contribution to Q from $\pm y$, and we write

$$Q(\theta) = \int_{y>0} K(\theta, y)\, g(y)\, \mathrm{d}y, \tag{24}$$

where

$$K(\theta, y) = K_+(\theta, y) + K_-(\theta, -y). \tag{25}$$

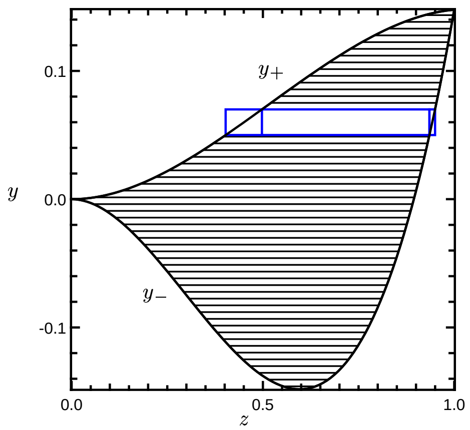

Figure 2. The region of integration in equation (20) for $\alpha = 0.5$, $\theta = \pi/3$ is bounded by the curved lines. For $g(y)$ piecewise constant it is convenient to split the integral into regions as shown by the boxes (here $y_j = 0.06$ and $\delta_j = 0.02$).

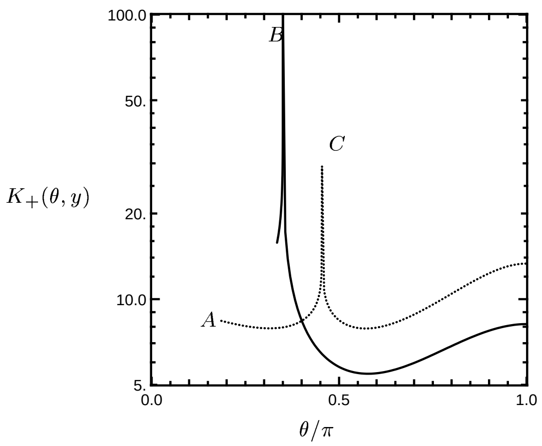

Figure 3. The function $K_+(\theta, y)$ for the two values of y corresponding to the orbits in Figure 1. The solid curve with the most pronounced spike is the thin orbit with $y/y_{\max} = 0.998$; the dotted curve with a lower, broader spike is the fat orbit with $y/y_{\max} = 0.462$. The symbols A and C mark the turning points of the fat orbit; B marks the ends of the thin orbit (cf. Figure 1).

The function $K(\theta, y)$ is illustrated in Figure 3 for two values of y. (The range of θ has been extended to $[0, \pi]$ for clarity. Thus, by equation (23), K_- can be read off from the $\theta > \pi/2$.) The banana shapes corresponding to these orbits are shown in Figure 1. The discontinuity and the cusp (A and C) correspond to the the top corner (A) and the bottom corner (C) of the fat banana in Figure 1. The end of the thin banana gives rise to similar features (B, cf. Figure 1) which are closer together. Since neither orbit is very sharply bent (cf. Figure 1), there is no contribution to K at small θ. In fact the only orbits which come near $\theta = 0$ (the minor axis) are fat ones—those with small y. The thinner orbit in Figure 1 does not contribute to the density at small θ. This illustrates that the thin shells cannot be arbitrarily sharply bent; i.e. all thin bananas subtend a finite angle.

3.4 Matrix formulation

Unfortunately, $y_\pm$ depend on z in such a non-trivial way that the integral over z in equation (20) cannot be simplified further analytically. But the integral over y can be done analytically for constant g, so our approximation will be to make a grid in y and make $g(y)$ piecewise constant on the grid; thus we set $g = g_j =$ constant for $y \in (y_j \pm \delta_j/2)$. We also need a set of values of $\theta = \theta_i$ at which to try and match the value of Q with that produced by our guess at g. Thus we recast equation (24) as a matrix equation:

$$Q_i = \sum_j K_{ij} g_j \tag{26}$$

with

$$K_{ij} = \int_{y_j-\delta_j/2}^{y_j+\delta_j/2} K(\theta_i, y)\, \mathrm{d}y. \tag{27}$$

We obtain

$$\begin{aligned} K_{ij} = \int \mathrm{d}z\, z^{1/\alpha-2} \times \\ \big\{ \sin^{-1} h(y_j+\delta_j/2) - \sin^{-1} h(y_j-\delta_j/2) \\ + \sin^{-1} h(-y_j+\delta_j/2) - \sin^{-1} h(-y_j-\delta_j/2) \big\}, \end{aligned} \tag{28}$$

where

$$h(y) = \begin{cases} 1, & y \ge y_+; \\ \dfrac{2(y-y_-)}{y_+-y_-} - 1, & y_- < y < y_+; \\ -1, & y_- \ge y. \end{cases} \tag{29}$$

with $y_\pm$ evaluated at (z, θ_i). With h defined this way, the limits of integration in equation (28) can be taken to be $(0,1)$, but it is more efficient numerically to split the interval into three parts according to the intersections of the strip $y \in (y_j \pm \delta_j/2)$ with $y_\pm$. An example is shown in Figure 2: the integration is carried out over each of the three boxes and the results added together.

To compute $Q(\theta)$ (equation 19), we need to compute the angular part of the density, $S(\theta)$. For our purposes it will suffice to expand S and P in a Fourier series and truncate at high order:

$$S(\theta) = \sum_{k=0}^{n} s_k \cos(k\theta) \tag{30}$$

$$P(\theta) = \sum_{k=0}^{n} p_k \cos(k\theta) \tag{31}$$

where p_k can be evaluated trivially from equations (2) and (7) by standard integrals, and

$$p_k = -s_k B\left(\tfrac{k+\alpha+1}{2}, \tfrac{1}{2}\right) B\left(\tfrac{k-\alpha}{2}, \tfrac{1}{2}\right) \tag{32}$$

(Kalnajs 1971, Syer and Tremaine 1996). Since $P(\theta)$ is not only even, but also symmetric about $\theta = \pi/2$, p_k and s_k vanish when k is odd. We truncate at $k = 30$, which leads to negligible error for $\alpha \ge 0.5$.

4 ANALYTIC RESULTS

A necessary condition for self-consistency is that the orbits can produce the flattening of the model. An indicator of the flattening is the ratio of Q on the minor axis to that on the major axis at the same radius. Namely

$$C \equiv \frac{Q(0)}{Q(\pi/2)}. \tag{33}$$

We can also define a similar quantity for each orbit y:

$$C_y \equiv \frac{K(0,y)}{K(\pi/2,y)}. \tag{34}$$

To make a self-consistent model, the value of C for the density must be within the range of the values given by the orbits: i.e.

$$\min[C_y] \le C(\alpha) \le \max[C_y], \tag{35}$$

for a self-consistent model with a potential cusp α. (*First mean value theorem*, inequality 12.111, Gradshteyn & Ryzhik 1980.)

The maximum of C_y is set by the fattest banana orbit ($y \to 0$), because it spends most of its time near apocentre, near the minor axis (cf. Figure 1). For such orbits,

$$C_y \to \max[C_y] = \begin{cases} \infty, & \alpha < \frac{1}{2}, \\ \frac{\Gamma\left(\alpha-\frac{1}{2}\right)\Gamma\left(\frac{1}{2}+\frac{\alpha}{2}\right)}{\Gamma(\alpha)\Gamma\left(\frac{\alpha}{2}\right)}. & \alpha > \frac{1}{2} \end{cases} \tag{36}$$

The minimum of the C_y occurs for the thinnest (closed) banana orbit ($y \to y_{\max}$). For such orbit, $C_y = \min[C_y] = 1/\sqrt{2}$. (See the Appendix for derivations of these limiting values of C_y.)

Figure 4 shows $C(\alpha)$ as a function of α. The inequality

$$\frac{1}{\sqrt{2}} \le C(\alpha) \le \max[C_y] \tag{37}$$

holds only for $\alpha \gtrsim 0.43$. So models with $0 < \alpha \lesssim 0.43$ cannot be made self-consistent. The inequality (35) is only a necessary condition for self-consistency, so models with higher α may or may not be self-consistent. Note, however, that $\max[C_y] \to 1$ *and* $C \to 1$ as $\alpha \to 1$, so (35) is only marginally satisfied. This may be a hint that it will be difficult to find self-consistent models for $\alpha \simeq 1$. To draw stronger conclusions we must try to solve equation (26) numerically.

To conclude the section on analytic results, we abandon for a moment the goal of self-consistency, and remark that when $g(y) =$ constant, Q is independent of θ. Thus $\Sigma \propto \Phi^{1-1/\alpha}$ and the contours of surface density coincide with the contours of the potential. As α approaches unity, Σ approaches a constant while Φ remains highly flattened. Intriguingly when $\alpha = 1$, $g(y) =$ constant is the trivial self-consistent solution. This model is however unphysical: Σ is constant but it vanishes for finite Φ.

5 NUMERICAL SOLUTIONS

The problem of finding self-consistent solution reduces to solving equation (26). A minimum requirement for a physical solution is that the solution $g(y)$ be positive definite. It should also be reasonably smooth.

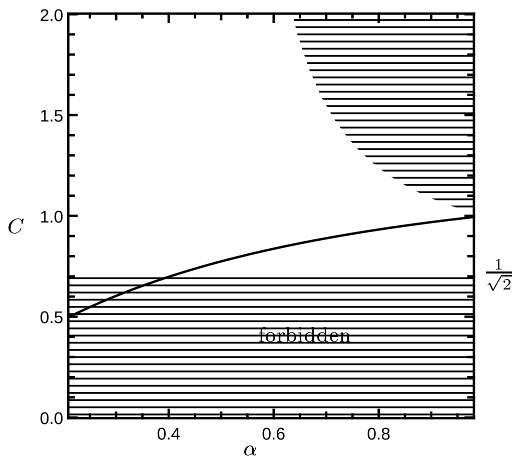

Figure 4. The ratio of the density at the minor axis vs that at the major axis for the Sridhar & Touma (1997) models. The shaded regions indicate those forbidden from self-consistency by inequality (35). Models with $C < 1/\sqrt{2}$ ($0 < \alpha \lesssim 0.43$) cannot be made self-consistent.

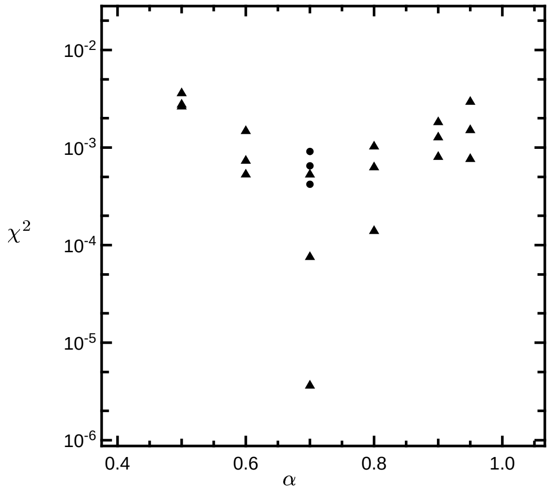

Figure 5. The residuals in the form of χ^2 of best fit orbit models as a function of α. Triangles are for $N_\theta = 11$, and circles for $N_\theta = 20$. From top to bottom in each case $N_y = [25, 50, 100]$. All models have significant residual ($\chi^2 \gg 10^{-12}$).

Thus we minimize the function

$$\chi^2 = \frac{1}{N_\theta} \sum_{i=1}^{N_\theta} \frac{\left[\left(\sum K_{ij} g_j\right) - Q_i\right]^2}{\sigma^2} + \lambda \mathcal{S}[g], \tag{38}$$

and require

$$g_j \geq 0, \qquad j \in [1, N_y]. \tag{39}$$

The smoothness is constrained through

$$\mathcal{S}[g] = (g_1 - g_2)^2 + (g_{N_y} - g_{N_y-1})^2 + \sum_{j=2}^{N_y-1} (2g_j - g_{j-1} - g_{j+1})^2 \tag{40}$$

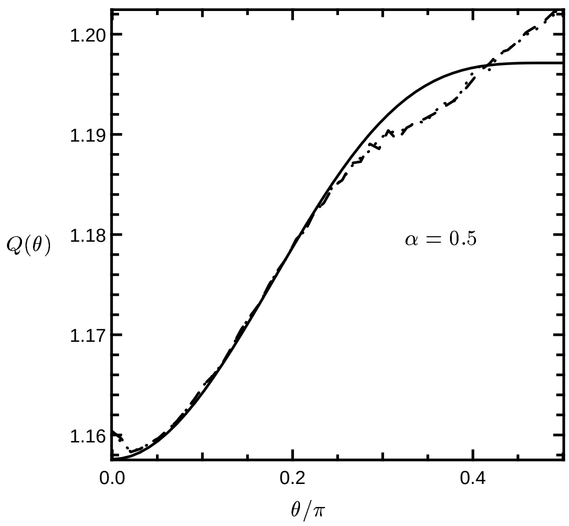

Figure 6. The target density Q (solid line) in the case $\alpha = 0.9$. The dashed line shows the best fit model with $(N_\theta, N_y) = (50, 100)$. The dotted line shows the best fit model with $(N_\theta, N_y) = (50, 200)$. The corresponding values of χ^2 are 0.0026 and 0.0023 respectively. In both cases $\lambda = 10^{-12}$, and consequently $g(y)$ is very far from smooth.

and a small tunable parameter λ. We set the characteristic scale for the deviation of the solution from the target to be

$$\sigma = Q(\frac{\pi}{2}) - Q(0). \tag{41}$$

This problem is solvable with standard routines such as QPROG of IMSL and E04NAF of NAG. A source code is in Hanson & Lawson (1995). Also an excellent general discussion of the method is in Press *et al.* (1992). We use a uniform grid in θ with $N_\theta = [11, 20, 50]$, and a logarithmic grid in y with $N_y = [25, 50, 100, 200]$. We apply a minimal smoothing constraint, $\lambda = 10^{-12}$ which leads to solutions with a large amount of structure on the smallest scales. Taken literally, this kind of distribution function is almost certainly unphysical, but it gives the most generous constraints on self-consistency: if we cannot find even highly oscillatory solutions, then smooth ones probably do not exist. We would consider models to be self-consistent if χ^2 was consistent with zero plus rounding error: i.e. $\chi^2 \leq 10^{-12}$.

Figure 5 shows the value of χ^2 for a range of models. Figure 4 suggests that self-consistency should be least constrained where the solid line is furthest from the forbidden regions. Hence we see in Figure 5 that the smallest value of χ^2 occurs for $\alpha \simeq 0.7$. Figure 5 also shows that additional resolution at $\alpha = 0.7$ gives larger values of χ^2 and thus provides a tighter constraint on self-consistency. None of the models has χ^2 consistent with zero.

We note that a more stringent test of self-consistency would perhaps be the maximum residual $\Delta_{\rm max}$ (as opposed to the mean square residual χ^2). From Figure 6 we see that typically the residuals cluster near one or both of the axes ($\theta = 0, \pi/2$). Thus $\Delta_{\rm max}$ can be much greater than $\sqrt{\chi^2}$.

5.1 Fricke expansion

To gain some insight to the source of non-self-consistency, we introduce a basis function approach to solving the Vlasov

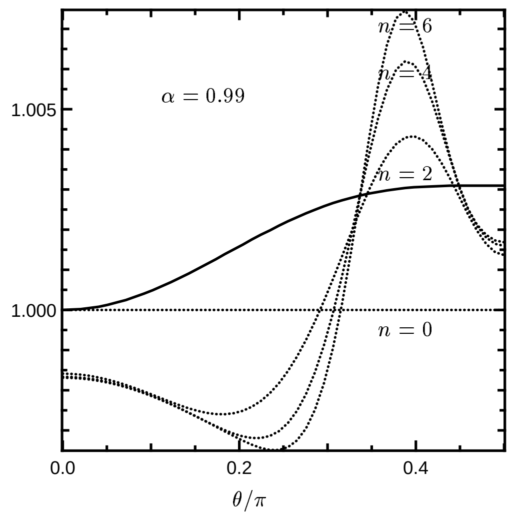

Figure 7. The target density Q (solid line) for $\alpha = 0.99$. Dotted lines are the contribution to Q from a distribution function with $g(y) = y^n$, for $n = [0, 2, 4, 6]$.

equation. Consider the distribution function obtained by setting $g(y) = y^n$ with n an integer. This is the equivalent of the method of expansion of a 3-d axisymmetric system due to Fricke (1951). Thus we set $g(y) = y^n$ in equation (20) and define

$$Q_n(\theta) = \int z^{1/\alpha-2} y^n \frac{\mathrm{d}z\mathrm{d}y}{\sqrt{(y-y_-)(y_+-y)}}. \tag{42}$$

If $g(y)$ is developed in a Taylor expansion about $y = 0$:

$$g(y) = \sum_n a_n\, y^n. \tag{43}$$

then $Q(\theta)$ is a Fricke expansion:

$$Q(\theta) = \sum_n a_n\, Q_n(\theta). \tag{44}$$

An expression for $Q_n(\theta)$ is derived in the Appendix. $Q_n(\theta)$ is plotted for $n = [0, 2, 4, 6]$, $\alpha = 0.99$ in Figure 7. All the Q_n with $n > 0$ have broadly similar shapes. They are flat for $\theta \gtrsim 0$ and have negative curvature; they rise and reach a maximum at around $\theta = 0.4\pi$; and they are all flat again at $\theta = \pi/2$. The maximum comes from adding up a series of cusps like the ones in Figure 3. Its position is fixed roughly by the minimum angle subtended by the thin bananas. The shape of the function Q, although it is very close to being constant, is rather different. We can understand broadly why the residuals in Figure 6 cluster at the axes. Given this, it looks rather unlikely that a Fricke expansion (44) of Q would converge.

To find the best fit Fricke expansion for a given model one can minimize the deviation of equation (44) from the true value of $Q(\theta)$ with respect to variations in a_n. In general it is difficult to control the values of a_n so as to keep $g(y)$ positive definite. For this reason we do not recommend Fricke expansion as a method of solving the Vlasov equation.

For $\alpha \simeq 1$ we know that $g(y)$ is approximately constant, so there is some hope that the a_n will be small for $n > 0$, and hence that $g(y)$ will remain positive. We tried fitting $Q(\theta)$ for $\alpha = 0.99$ with a Fricke expansion. Very poor fits result up to $n = 14$, and are improved very little by going to $n = 22$. The corresponding $g(y)$ turns out not to be positive definite, and it is highly oscillatory (more so for the higher order fit, showing the non-convergent nature of the expansion).

6 CONCLUSIONS

We attempt to build self-consistent models for the sequence of Stäckel potentials of Sridhar & Touma (1997). Our numerical solutions suggest that such models do not exist for the whole range of $0 < \alpha < 1$. We also found a simple analytic argument to show that models with $0 < \alpha \lesssim 0.43$ cannot be self-consistent: all orbits put too much mass near the minor axis of the potential, and too little mass near the major axis. Unfortunately the argument does not apply to higher α.

We only considered the scale-free models of Sridhar & Touma (1997). There are two important generalizations which are not scale free: those with central black holes, and those which are linear superpositions of models with $\alpha \in (0, 1)$. Consider first a black hole model consisting of a model with $\alpha \in (0, 1)$ but including a black hole of mass M. (The black hole component can be thought of as a model with $\alpha = -1$.) Close to the black hole there are lens orbits in addition to the bananas, and there is a chance that a model composed largely of lenses could be self-consistent (Sridhar & Touma 1997). However, at large radius the black hole is insignificant, and the system should approach the scale-free case. To be more precise, as $r \to \infty$ a diminishing fraction of phase space will be taken up with lenses (those with $y \simeq 0$). This fact by itself is not sufficient to *prove* that the models can not be made self consistent, but it is highly restrictive, and we expect self-consistent models to face the same difficulties as in the present work. Simple linear superpositions of a finite number of models with $\alpha \in (0, 1)$ will have similar asymptotic problems.

Our results show that regular orbits in a particular set of cuspy non-axisymmetric potentials do not have enough freedom to make a self-consistent model. The models we study are 2-dimensional, but because of their low symmetry they are analogous to triaxial systems. Had self-consistent models been found it would have been an interesting counter argument against the conclusions of existing work on triaxial cusps and galactic nuclei. In fact, we are in agreeement with the conclusions of Merritt & Fridman (1996) with respect to a rather different potential set. In this case the conclusion was that the box orbits required to build non-axisymmetric models are made stochastic by the central cusp. In contrast, the potentials we use do not admit stochastic orbits, and yet still no self-consistent equilibria were found. In our opinion, doubt is cast on the existence of triaxial galactic nuclei by this result.

There are two caveats. We cannot rule out the existence of nearby equilibria—with density profiles very close to the one studied here but containing some stochastic orbits. Also, our result really only applies to self-gravitating star clusters, or equivalently far away from a central black hole. These questions are however beyond the scope of the present work.

Acknowledgments: we acknowledge interesting and useful discussions with S. Sridhar, Tim de Zeeuw and Scott Tremaine. The authors are grateful for hospitality provided by their irrespective institutions and to EARA for facilitating the exchange.

REFERENCES

Bishop J.L. 1987, ApJ, 322, 618

Crane, P., *et al.* 1993, AJ, 106, 1371

Dubinski, J., & Carlberg, R.G., 1991, ApJ, 378, 496

Franx M., Illingworth G. & de Zeeuw T.P. 1991, ApJ, 383, 112

Gebhardt K. et al. 1996, AJ, 112, 105

Fricke, W. 1951, *Astron. Nachr.*, 280, 193 (in German)

Gradshteyn, I.S. & Ryzhik, I.M. 1980, *Table of Integrals, Series and Products, 4th ed.*, New York: Academic Press.

Hanson, R.J. & Lawson, C.L. 1995, *Solving Least Squares Problems*, Classics in Applied Mathematics, (Philadelphia: SIAM)

Kalnajs, A.J. 1971, ApJ, 166, 275

Kuijken K. 1993, ApJ, 409, 68

Merritt D. & Fridman T. 1996, ApJ, 460, 136

Merritt D. 1996, AJ, 112, 1085

Navarro J., Frenk C. & White S. 1996, ApJ, 462, 563

Press, W.H., Teukolsky, S.A., Vetterling, W.T., and Flannery, B.P. 1992, *Numerical Recipes*, Cambridge: Cambridge University Press.

Schwarzschild M. 1993, ApJ, 409, 563

Sridhar S. & Touma J. 1997, MNRAS, 287, L1

Statler T.S., 1994, ApJ, 425, 458

Syer D. & Tremaine S. 1996, MNRAS, 281, 925

van Albada, T.S. 1982, MNRAS, 201, 939

APPENDIX

Definition of $y_\pm$

The boundary of the region of integration in equation (20) is defined by the quantities

$$\begin{aligned} y_- &= -uz^{1/\alpha}(1-u^\alpha z), \\ y_+ &= vz^{1/\alpha}(1-v^\alpha z), \end{aligned} \tag{45}$$

where

$$\begin{aligned} (u,v) &= (\xi,|\eta|)\,\Phi^{-\frac{1}{\alpha}} \\ &= (1+\cos\theta, 1-\cos\theta)\;P(\theta)^{-\frac{1}{\alpha}}. \end{aligned} \tag{46}$$

From equations (2) & (7) it follows that $P(\theta) \geq P(\pi/2) = 1$, $u(\theta) \geq u(0) = u(\pi/2) = 1$ and $v \in (0,1)$.

Limiting values of C_y

Next we derive the value of C_y (equation 34) for the limiting cases $y \to 0$ and $y \to y_{\rm max}$.

At $\theta = 0$ we have $(u,v) = (1,0)$ and $y_+ = 0$ while $-y_- = x(z)$ where

$$x(z) \equiv z^{1/\alpha}(1-z). \tag{47}$$

Thus $K_+ = 0$ and

$$\begin{aligned} K(0,y) &= K_-(0,-y) \\ &= \frac{1}{\sqrt{y}}\int z^{1/\alpha-2}\frac{{\rm d}z}{\sqrt{x-y}}. \end{aligned} \tag{48}$$

At $\theta = \pi/2$ we have $u = v = 1$ and $y_+ = -y_- = x$. Thus $K_- = K_+$ and

$$\begin{aligned} K(\pi/2,y) &= 2K_+(\pi/2,y) \\ &= 2\int z^{1/\alpha-2}\frac{{\rm d}z}{\sqrt{(x-y)(x+y)}}. \end{aligned} \tag{49}$$

As $y \to 0$ the numerator in (49) diverges at $z = y$. Thus the value of the integral is dominated by the contribution from $z \simeq 0$, and we can replace x by $z^{1/\alpha}$. Changing variable to $w = z^{1/\alpha}/y$, we obtain

$$K(\pi/2,y) \to 2\alpha y^{-\alpha}\int\frac{w^{-\alpha}{\rm d}w}{\sqrt{w^2-1}}, \tag{50}$$

whence, extending the limits of integration to $[1,\infty)$,

$$K(\pi/2,y) \to y^{-\alpha}\alpha\sqrt{\pi}\frac{\Gamma\left(\frac{\alpha}{2}\right)}{\Gamma\left(\frac{1+\alpha}{2}\right)}, \qquad \text{as} \quad y \to 0. \tag{51}$$

This expression is valid for $\alpha > 0$, but for $\alpha \simeq 0$ it is not very accurate. This can be rectified by adding the next highest order (logarithmic) term:

$$K(\pi/2,y) \to \alpha y^{-\alpha}\sqrt{\pi}\frac{\Gamma\left(\frac{\alpha}{2}\right)}{\Gamma\left(\frac{1+\alpha}{2}\right)} + 2(1+\alpha)\ln\frac{1}{y}. \tag{52}$$

For $\alpha < \frac{1}{2}$, as $y \to 0$, the integral in equation (48) converges, so:

$$K(0,y) \to \sqrt{\frac{\pi}{y}}\,\frac{\Gamma\left(\frac{1}{2\alpha}-1\right)}{\Gamma\left(\frac{1}{2\alpha}-\frac{1}{2}\right)}, \qquad \text{as} \quad y \to 0. \tag{53}$$

For $\alpha > \frac{1}{2}$, the same trick of replacing x by $z^{1/\alpha}$ works, and we obtain

$$K(0,y) \to y^{-\alpha}\alpha\sqrt{\pi}\frac{\Gamma\left(\alpha-\frac{1}{2}\right)}{\Gamma\left(\alpha\right)}. \tag{54}$$

Thus

$$C_y \to \begin{cases} \dfrac{y^{\alpha-\frac{1}{2}}}{\alpha}\dfrac{\Gamma\left(\frac{1}{2\alpha}-1\right)\Gamma\left(\frac{1}{2}+\frac{\alpha}{2}\right)}{\Gamma\left(\frac{1}{2\alpha}-\frac{1}{2}\right)\Gamma\left(\frac{\alpha}{2}\right)}, & \alpha < \frac{1}{2}, \\ \dfrac{\Gamma\left(\alpha-\frac{1}{2}\right)\Gamma\left(\frac{1}{2}+\frac{\alpha}{2}\right)}{\Gamma(\alpha)\Gamma\left(\frac{\alpha}{2}\right)}, & \alpha > \frac{1}{2}, \end{cases} \tag{55}$$

as $y \to 0$. This is the maximum value of C_y.

As $y \to y_{\rm max}$, $x \to y$, and we can set everything in the integrands for $K_\pm$ constant, except $\sqrt{x-y}$. Hence

$$K(0,y) \to \frac{z_{\rm max}^{1/\alpha-2}}{\sqrt{y_{\rm max}}}\int\frac{{\rm d}z}{\sqrt{x-y}}, \tag{56}$$

and

$$K(\pi/2,y) \to \sqrt{2}\,\frac{z_{\rm max}^{1/\alpha-2}}{\sqrt{y_{\rm max}}}\int\frac{{\rm d}z}{\sqrt{x-y}}. \tag{57}$$

Thus

$$C_y \to \frac{1}{\sqrt{2}}, \qquad \text{as} \quad y \to y_{\rm max}. \tag{58}$$

This is the minimum value of C_y.

Coefficients of Fricke expansion

We derive an expression for $Q_n(\theta)$ (equation 44). First we define

$$\begin{aligned} \bar{y} &= \tfrac{1}{2}(y_+ + y_-) \\ \Delta &= \tfrac{1}{2}(y_+ - y_-), \end{aligned} \tag{59}$$

and then set

$$y = \bar{y} - \Delta\sin\beta \tag{60}$$

in equation (42). We write

$$Q_n = \sum_{m=0}^{n} q_{mn} \int z^{1/\alpha-2}(y_+ + y_-)^{n-m}(y_+ - y_-)^m \, \mathrm{d}z. \quad (61)$$

Since $g(y)$ is even in y we restrict our attention to even n. In this case the result is

$$q_{mn} = \begin{cases} 2^{1-n} \binom{n}{m} \int\limits_0^{\pi/2} \sin^m \beta \, \mathrm{d}\beta, & \text{for even } m; \\ 0, & \text{otherwise.} \end{cases} \quad (62)$$

Using standard integrals:

$$q_{mn} = \binom{n}{m} \frac{\sqrt{\pi}}{2^n} \frac{\Gamma\left(\frac{1+m}{2}\right)}{\Gamma\left(1+\frac{m}{2}\right)} \quad (63)$$

for even m. In principle the integral in equation (61) is also analytic, since (n, m) are integers.

This paper has been produced using the Royal Astronomical Society/Blackwell Science TEX macros.